Title

Atmospheric sulfur isotopic anomalies recorded at Mt. Everest across the Anthropocene

Journal

Proceedings of the National Academy of Sciences of the United States of America, 115(27)

ISSN

0027-8424

Authors

Lin, Mang
Kang, Shichang
Shaheen, Robina
et al.

Publication Date

2018-07-03

DOI

10.1073/pnas.1801935115

Peer reviewed

Atmospheric sulfur isotopic anomalies recorded at Mt. Everest across the Anthropocene

Mang Lin[a,b,1,2], Shichang Kang[c,d,e], Robina Shaheen[a], Chaoliu Li[d,f], Shih-Chieh Hsu[b,3], and Mark H. Thiemens[a,1]

[a]Department of Chemistry and Biochemistry, University of California, San Diego, La Jolla, CA 92093; [b]Research Center for Environmental Changes, Academia Sinica, Taipei 115, Taiwan; [c]State Key Laboratory of Cryospheric Sciences, Northwest Institute of Eco-Environment and Resources, Chinese Academy of Sciences, 730000 Lanzhou, China; [d]Center for Excellence in Tibetan Plateau Earth Sciences, Chinese Academy of Sciences, 100101 Beijing, China; [e]University of Chinese Academy of Sciences, 100049 Beijing, China; and [f]Key Laboratory of Tibetan Environment Changes and Land Surface Processes, Institute of Tibetan Plateau Research, Chinese Academy of Sciences, 100101 Beijing, China

Edited by Barbara J. Finlayson-Pitts, University of California, Irvine, CA, and approved May 17, 2018 (received for review February 2, 2018)

Increased anthropogenic-induced aerosol concentrations over the Himalayas and Tibetan Plateau have affected regional climate, accelerated snow/glacier melting, and influenced water supply and quality in Asia. Although sulfate is a predominant chemical component in aerosols and the hydrosphere, the contributions from different sources remain contentious. Here, we report multiple sulfur isotope composition of sedimentary sulfates from a remote freshwater alpine lake near Mount Everest to reconstruct a two-century record of the atmospheric sulfur cycle. The sulfur isotopic anomaly is utilized as a probe for sulfur source apportionment and chemical transformation history. The nineteenth-century record displays a distinct sulfur isotopic signature compared with the twentieth-century record when sulfate concentrations increased. Along with other elemental measurements, the isotopic proxy suggests that the increased trend of sulfate is mainly attributed to enhancements of dust-associated sulfate aerosols and climate-induced weathering/erosion, which overprinted sulfur isotopic anomalies originating from other sources (e.g., sulfates produced in the stratosphere by photolytic oxidation processes and/or emitted from combustion) as observed in most modern tropospheric aerosols. The changes in sulfur cycling reported in this study have implications for better quantification of radiative forcing and snow/glacier melting at this climatically sensitive region and potentially other temperate glacial hydrological systems. Additionally, the unique $\Delta^{33}S$–$\delta^{34}S$ pattern in the nineteenth century, a period with extensive global biomass burning, is similar to the Paleoarchean (3.6–3.2 Ga) barite record, potentially providing a deeper insight into sulfur photochemical/thermal reactions and possible volcanic influences on the Earth's earliest sulfur cycle.

Himalayas | mass-independent fractionation | aerosol | glacier | Archean

The Himalayas and Tibetan Plateau (HTP), the largest and highest plateau on the Earth, is climatically unique and important due to its location, topography, and teleconnection with other parts of the world (1). It hosts the largest number of glaciers outside the polar regions and thousands of lakes, and is commonly referred to as the "Third Pole." The ice and lake sediment cores from this midlatitude region provide valuable paleoclimatic and paleoatmospheric records that cannot be obtained from polar regions (2–5). The HTP is also known as the "Asian water tower" because snow and glacier melting in this region sustains water availability for major rivers in Asia and sustenance for >1.4 billion people (6). A persistent increase in aerosol loading over this region has been altering the atmospheric/glacial chemical composition, snow/glacier melting rate, and glacial river water quality (3, 6, 7). Sulfate is one of the major components of aerosols (especially in Asia), but the relative contributions of varying sources (e.g., combustion, mineral dust) and its mixing state in aerosols remain uncertain because measurements of source-specific tracers in sulfates are absent. This fragmentary understanding limits our ability to accurately quantify the aerosol budget and evaluate its influences on climate and hydrological systems.

The sulfur isotopic anomaly (or mass-independent fractionation [MIF]) is quantified by nonzero $\Delta^{33}S$ and $\Delta^{36}S$ values, where $\Delta^{33}S = \delta^{33}S - 1{,}000 \times [(1 + \delta^{34}S/1{,}000)^{0.515} - 1]$ and $\Delta^{36}S = \delta^{36}S - 1{,}000 \times [(1 + \delta^{34}S/1{,}000)^{1.9} - 1]$ (*Materials and Methods*). In the modern atmosphere, sulfate emitted from combustion and secondarily produced from photolytic oxidation of stratospheric SO_2 are the only two known types of isotopically anomalous sulfates (8–12). Other sulfates (e.g., terrigenous sulfate in mineral dust, secondary sulfate produced in the troposphere via SO_2 oxidation) are all isotopically normal ($\Delta^{33}S \sim 0‰$) (8–13). This unique isotopic fingerprinting has been utilized in reconstructing changes in sources and chemical formation pathways of sulfur in the past atmosphere using ice/snow samples obtained from polar regions (11, 14), but the difficulty of drilling ice cores at Himalayas in terms of the harsh environment at high altitudes (>6,500 m above sea level) (2, 5) hampers such studies in this region. Here we provide multiple sulfur isotopic analysis spanning over 200 y in a Himalayan lake sediment core (*Materials and*

Significance

Signatures of sulfur isotopic anomalies (a proxy used in tracking the atmospheric oxygen/sulfur cycles in the past) preserved in the Himalayas ("Asian water towers") reveal significant changes in the regional atmospheric sulfur cycle and glacial hydrological system during the second industrial revolution. The record extends our atmospheric sulfur isotopic anomaly observation to a unique region and different time and transitional period. Distinct from most existing aerosol measurements made in the twenty-first century, the 200-y record mimics the Archean (4–2.5 billion years ago) barite record and may provide a broader view of the mechanistic origin of sulfur isotopic anomalies in the modern atmosphere and another tool to deepen insights into the Earth's sulfur cycle during the evolution of early life.

Author contributions: M.L., R.S., and M.H.T. designed the sulfur isotopic study; M.L. and S.K. collected aerosol, glacial snow, and river samples; S.K. and C.L. collected sediment samples; S.K., C.L., and S.-C. H. proposed elemental and lead isotopic measurements; M.L. performed isotopic and elemental measurements; M.L. analyzed data; M.L., S.K., and M.H.T. interpreted results; and M.L., R.S., and M.H.T. wrote the paper.

The authors declare no conflict of interest.

This article is a PNAS Direct Submission.

[1]To whom correspondence may be addressed. Email: manglin.ucsd@gmail.com or mthiemens@ucsd.edu.

[2]Present address: School of Materials and Chemical Technology, Tokyo Institute of Technology, 266-8502 Yokohama, Japan.

[3]Deceased October 10, 2014.

This article contains supporting information online at www.pnas.org/lookup/suppl/doi:10.1073/pnas.1801935115/-/DCSupplemental.

Published online June 18, 2018.

Methods) to gain insight into the change of sulfur source in this climatically sensitive and important region. As a part of the world's highest freshwater lake system, this remote lake is significantly different from many saline lakes on the HTP (15). The low background sulfate concentration and low biological activity (i.e., minimal postdepositional processes) (16) renders this alpine lake an ideal site to reconstruct regional atmospheric sulfur cycle and potentially to record climate-induced changes in weathering/erosion within the glacial hydrological system.

Atmospheric Sulfur Isotopic Compositions in the Central HTP

We first report $\Delta^{33}S$ (and $\Delta^{36}S$) values in sulfate aerosols [in total suspend particles (TSP)] collected at the central HTP (*Materials and Methods* and *SI Appendix*, Fig. S1) to gain an overview of the atmospheric sulfur isotopic anomalies in this arid region (Fig. 1). Because mineral dust or local soil accounts for ~3/4 of TSP at our sampling site in today's environment (17) and sulfate derived from this terrigenous source is isotopically normal ($\Delta^{33}S$ = 0‰), the observed $\Delta^{33}S$ values (ranging from 0.05‰ to 0.12‰) are less than most sulfate aerosols collected at midlatitudes (8–10). A first-order estimation based on isotopic mass balance (*SI Appendix*) yields a $\Delta^{33}S$ value of nondust sulfate to be 0.36 ± 0.12‰. This estimation is at the higher end of the $\Delta^{33}S$ range of currently measured tropospheric sulfate aerosols (maximum: 0.53‰) (8–10), likely because the HTP is frequently affected by the downward transport of stratospheric air (18, 19), which contains stratsopheric sulfates with positive $\Delta^{33}S$ values (8–10). Such a large anomaly cannot be explained by small variations of $\Delta^{33}S$ (±0.1‰) led by slight differences in mass-dependent fractionation (MDF) exponents ($^{33}\theta$) of varying SO_2 oxidation pathways in the troposphere (13). The scattered $\Delta^{33}S$–$\Delta^{36}S$ relationship observed in aerosols collected from Beijing and California (La Jolla, Bakersfield, and White Mountain) (Fig. 1) indicates that at least two types of isotopically anomalous sulfates (produced in the stratosphere by photolytic oxidation processes and emitted from combustion) may affect $\Delta^{36}S/\Delta^{33}S$ slopes in differing ways. If this is the case, the relatively well-defined $\Delta^{36}S/\Delta^{33}S$ slope (−1.80 ± 0.85, n = 6) observed in this study (Fig. 1), close to that of stratospheric sulfates estimated from polar records of stratospheric volcano eruptions (−1.93 ± 0.62, n = 13) (14), may imply that the central HTP is predominately affected by a single sulfur isotopic anomaly source (likely stratospheric sulfates) in the twenty-first century.

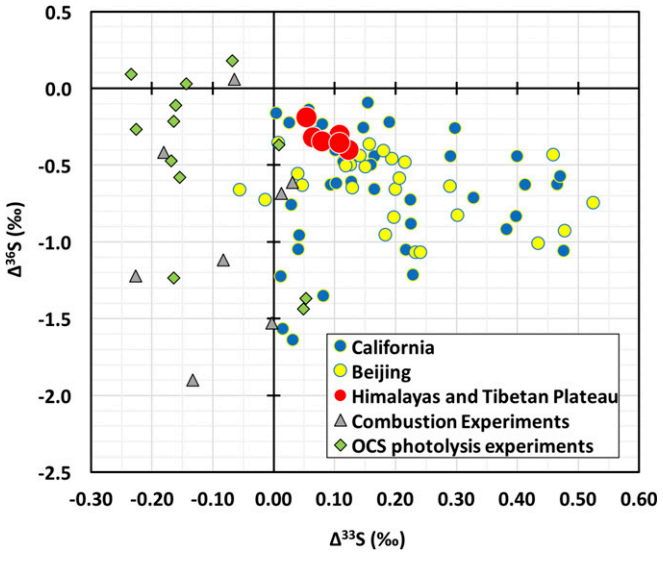

Fig. 1. The $\Delta^{33}S$ and $\Delta^{36}S$ in sulfate aerosols collected at the HTP; $\delta^{34}S$ values (ranging from 3.0‰ to 6.7‰) are reported in *SI Appendix*. The $\Delta^{33}S$ and $\Delta^{36}S$ values of tropospheric sulfate aerosols collected at California (8) and Beijing (9), primary sulfate aerosols emitted from biomass and fossil fuel combustion experiments (12), elemental sulfur produced from OCS photolysis experiments (47) are also shown in this figure.

Two-Century Record of Atmospheric Sulfur Isotopic Anomalies

The sulfur isotopic analysis of post-1930 lake sediments (n = 8) display zero $\Delta^{33}S$ values within analytical error (±0.01‰) (Fig. 2*A* and *Materials and Methods*), likely a result of a larger contribution of mineral dust to TSP in the Himalayas than the central HTP as noted by previous aerosol and ice core studies (4, 20) and in part supported by near-zero $\Delta^{33}S$ values in glacial snow and river sulfates (0.03‰ and 0.02‰, respectively) collected at the Mt. Everest in this study (*SI Appendix*). The isotopically normal sulfates may also originate from the weathering process of parent rocks, which is supported by (*i*) the low enrichment factors of major, trace, and rare earth elements, and (*ii*) the observed stable lead isotopic composition ($^{206}Pb/^{207}Pb$ and $^{208}Pb/^{207}Pb$) that is nearly identical to soils and river sediments over the HTP (21, 22) (*SI Appendix*, Figs. S2 and S3).

In contrast, most sulfate samples (six of eight) deposited in the pre-1930 period display small but distinguishable nonzero $\Delta^{33}S$ values (> ±0.02‰, at the 2σ level) (Fig. 2*A*), which may not be an analytical artifact because multiple laboratory controls throughout the study period show that the measured $\Delta^{33}S$ values are highly reproducible (*SI Appendix* and *SI Appendix*, Table S1). Even if the mass-dependent field is defined as ±0.05‰ (at the 5σ level), two samples in the nineteenth century (1818–1853 and 1885–1886) still possess nonzero $\Delta^{33}S$ values. In this study, we attempted to extract acid volatile sulfide [(AVS) reduced forms of sulfur] (*SI Appendix*), but none of our sediment samples contain AVS. The absence of AVS suggests that microbial sulfur reduction processes are negligible in this oligotrophic lake (15) due to insufficient supply of organic matter (16). Subsequently, the observed nonzero $\Delta^{33}S$ values, particularly in two samples in the nineteenth century (1818–1853 and 1885–1886), could not be explained by the slight differences in MDF exponents in various microbial sulfur reduction/disproportionation processes and mixing of various sulfur reservoirs, as those observed in geological samples of Phanerozoic age (23, 24). This interpretation is further supported by the small $\delta^{34}S$ variation in our sedimentary sulfates (Fig. 2*B*) and zero $\Delta^{33}S$ values (within ±0.01‰) in all post-1930 samples. We therefore suggest that the origin of the relatively large anomalies in the 1818–1853 and 1885–1886 samples, if not all statistically resolvable anomalies, is attributed to MIF signatures in atmospheric sulfates deposited in lake sediments.

The long-term variations in sulfate concentrations recorded in the Himalayan lake sediment (Fig. 2*C*) match the inventory of global anthropogenic sulfur emissions (5, 25). The most striking finding of this study is that nonzero $\Delta^{33}S$ values are not observed after the second industrial revolution, when sulfate concentrations started to rise (>0.5 μg mg^{-1}) (Fig. 2 *A* and *C*). This observation is in marked contrast to nonzero $\Delta^{33}S$ values in most existing aerosol measurements made in the twenty-first century (8–10). Simultaneous increasing trends for Hg, U, Mo, Sb, and Tl in the same sediment core and atmospheric CO_2 mixing ratios (Fig. 3) also indicate that the increased sulfates are likely anthropogenic, but the absence of sulfur isotopic anomaly provides strong observational evidence that sulfate emitted from combustion (or produced from photolytic oxidation of stratospheric SO_2) is a highly unlikely source because they possess nonzero $\Delta^{33}S$ values as observed at two sides of the Pacific Ocean (8–10), the South Pole (11), and controlled combustion experiments in a chamber (12). As discussed, the Himalayas are strongly affected by dust aerosols (4, 20), and the increased sulfate is therefore likely attributed to two types of dust-associated sulfate aerosols

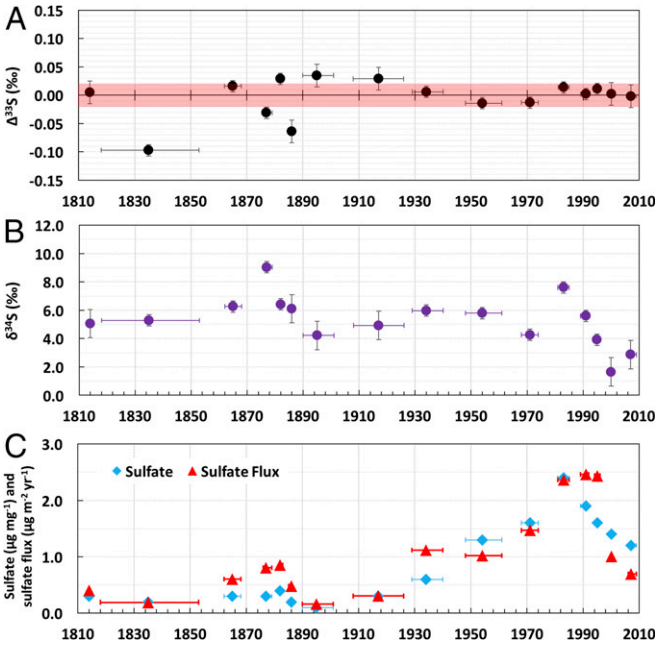

Fig. 2. Time series of (*A*) $\Delta^{33}S$, (*B*) $\delta^{34}S$, and (*C*) sulfate concentration and flux. Note that horizontal bars represent time intervals of combined sediment samples instead of dating errors. The ^{210}Pb-dated age was reported by Kang et al. (3). Vertical errors bars represent one SD uncertainties made on the basis of reproducibility of the laboratory standard with varying sample sizes (*Methods and Materials*). The red shaded area between −0.02‰ and 0.02‰ in *A* represents the mass-dependent field. Points distinguished from this field are interpreted to be sulfur isotopic anomalous (see *Materials and Methods* for details).

($\Delta^{33}S \sim 0‰$): (*i*) secondary sulfate produced from transition metal ion catalysis or O_3 oxidation of anthropogenic emitted SO_2 on the surface of mineral dust (26, 27), and/or (*ii*) terrigenous sulfate in anthropogenic emission of mineral particles from South Asia (*SI Appendix*, Fig. S1) (28). Another important source of isotopically normal sulfate that diluted/overprinted the MIF signature is strong weathering/erosion in this Himalayan glacial hydrological system in the twenty-first century as revealed by various weathering indices and Hf in the same sediment core (Fig. 3 and *SI Appendix*, Fig. S4), which is linked to pronounced warming trends, enhanced precipitation, and glacier melting (29–31). Our interpretation is independently supported by results from the positive matrix factorization (PMF) model (a receptor model widely used for source apportionment; https://www.epa.gov/air-research/positive-matrix-factorization-model-environmental-data-analyses) based on major, trace, and rare earth element measurements in the same sediment core (*SI Appendix*): the relative background contribution decreased from 65 ± 20% in the pre-1930 period to 10 ± 11% in the post-1930 period; relatively contributions of anthropogenic influences and weathering/erosion (14 ± 9% and 20 ± 14%, respectively) in the pre-1930 period enhanced to 45 ± 14% and 45 ± 10%, respectively, in the post-1930 period (*SI Appendix*, Figs. S5 and S6).

Possible Origins of Negative $\Delta^{33}S$ Values

Three samples in the nineteenth century possess negative $\Delta^{33}S$ values (< −0.02‰) and the largest anomaly ($\Delta^{33}S = -0.10 \pm 0.01‰$) is found in sulfates deposited from ∼1818 to ∼1853 (Fig. 2*A*). The negative values are surprising in that they contrast with positive $\Delta^{33}S$ values in most sulfate aerosols (101 of 118) collected at midlatitudes (including the HTP) in the twenty-first century (Fig. 4). Large positive $\Delta^{33}S$ values found in sulfates produced from laboratory SO_2 photochemistry experiments (in the presence of O_2) (32) indicate that the observed positive $\Delta^{33}S$ values in most tropospheric sulfate aerosols are likely attributed to the frequent downward transport of stratospheric sulfates at midlatitudes, which have been noted by previous studies (8–10). However, negative $\Delta^{33}S$ values measured in this study and recently observed in urban Beijing during a highly polluted season with active industrial/residential coal combustion and minimal stratospheric influences (−0.21 ± 0.19‰; minimum: −0.66‰) (10) are not expected, indicating that an additional MIF process may be required.

Combustion is a highly likely candidate (10, 11) because negative $\Delta^{33}S$ values (minimum: −0.23‰) have been observed in the primary sulfates emitted from combustion in controlled chamber experiments of biomass and diesel fuels (12) (Fig. 1). The fundamental chemical physics remain inadequately described, but recombination of elemental sulfur shown in a recent theoretical study (33) is the most likely mechanism based upon the isoelectronic reactions of sulfur species that mimic the well-known ozone formation reaction where the first chemically produced MIF anomalies were observed as a result of symmetry effects (34, 35). A number of radical driven reactions (e.g., $SH + H \rightarrow S + H_2$, $SH + SH \rightarrow S + H_2S$, $S + SH \rightarrow S_2 + H$) in combustion plumes (especially biomass burning) (36, 37) potentially produce elemental sulfur allotropes (e.g., S and S_2) at these high molecule number densities. These reactions, based upon gas phase recombination reaction theory and symmetry effects (33), are likely mass independent. Laboratory experiments have shown that symmetry reactions in sulfur-bearing species produce sulfur MIF isotopic compositions (38). Further laboratory investigation and field-based measurements of both $\Delta^{33}S$ and $\Delta^{36}S$ along with combustion tracers in the future are crucial to examine the extent to which recombination reactions (33) in combustion processes affect the signature of sulfur

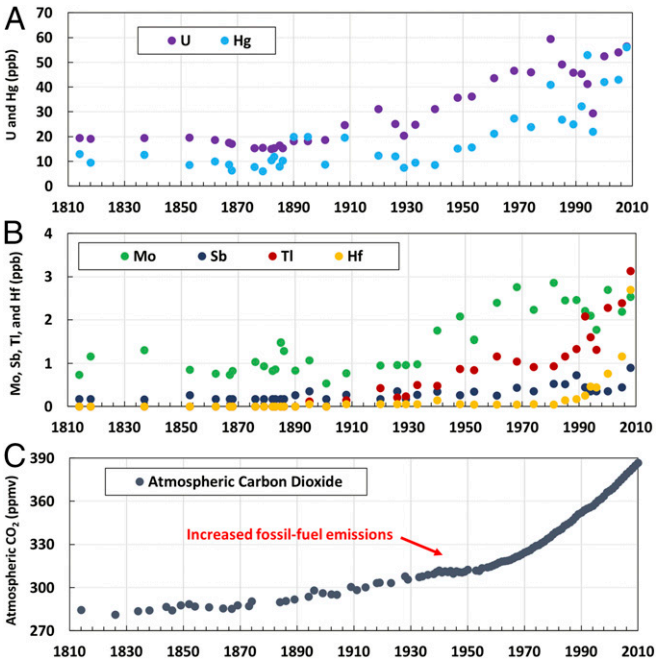

Fig. 3. Time series of (*A*) U and Hg, and (*B*) Mo, Sb, Tl, and Hf. The ^{210}Pb-estimated age and Hg concentrations were obtained from Kang et al. (3). These elements are selected out of 49 measured elements because their concentration ratios of the post-1930 to pre-1930 periods are greater than 2. (*C*) Time series of atmospheric CO_2 record (Scripps CO_2 Program: scrippsco2.ucsd.edu/) based on ice core data and direct observation from Mauna Loa and the South Pole.

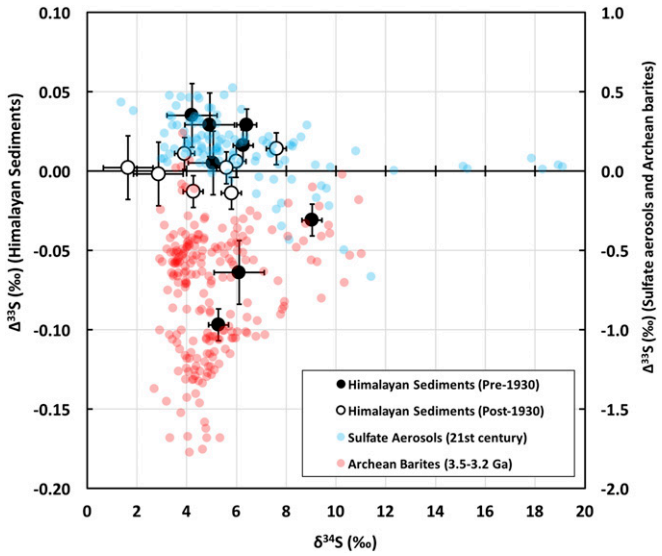

Fig. 4. Stable sulfur isotopic compositions in sulfates extracted from the Himalayan sediment core, modern aerosols, and Archean barites. Modern aerosol data (blue) is obtained from this study and refs. 8–10. The Archean barite data (red) is obtained from refs. 50–58. Note that the $\Delta^{33}S$ values for sediment samples are one order of magnitude smaller than aerosol and barite data because the signature of sulfur isotopic anomaly is greatly diluted by isotopically normal sulfates as discussed in the main text.

isotopic anomalies in emitted sulfates on experimental and observational basis, respectively.

Global lake sedimentary charcoal records, including the one retrieved from the southeast HTP (*SI Appendix*, Fig. S7), have shown that the nineteenth century is a period with extensive biomass burning around the globe, especially in the northern hemisphere extratropics (39, 40). Although black carbon records in the central HTP showed that biomass burning activities after the late twentieth century may be stronger than the nineteenth century (41), impacts of large-scale fires in the nineteenth century (likely attribute to land-clearing processes as a result of rapid population growth) (40) on sulfur partitioning (in isotopes and species) are probably different from small-scale biomass burning after the late twentieth century (as a consequence of fire suppression management policy, decreased vegetation density, and forest fragmentation) (39, 40). In large and persistent biomass-burning plumes, high molecule number densities of S and S_2 occur, and therefore isotopically anomalous sulfates may be directly emitted from combustion plumes (12) via the mechanism discussed earlier, and responsible for the negative $\Delta^{33}S$ values observed in our sediment core. The biomass-burning end member of $\Delta^{33}S$ was not unambiguously identified in the early combustion experiments (12), and further investigation is required. Here we provide a first-order estimation. Given that anthropogenic sulfur emissions before 1850 are dominated by grassland and forest fires (25), we assume that the PMF-model–estimated anthropogenic influence in the 1818–1853 period ($15 \pm 5\%$) (*SI Appendix*, Fig. S6), when the most negative $\Delta^{33}S$ value (−0.10‰) is observed, is exclusively attributed to biomass burning. Based on isotopic mass balance (*SI Appendix*), a biomass-burning end member of $\Delta^{33}S$ is determined to be -0.67 ± 0.20‰. This first-order estimation independently agrees well with the most negative $\Delta^{33}S$ value (−0.66‰) observed in Beijing during heavy pollution events (10).

Another possible influence of biomass burning in the production of sulfur isotopic anomalies is the stratospheric photochemistry of carbonyl sulfide (OCS). With biomass burning as one of its major sources, OCS is the most abundant sulfur-bearing molecule in the terrestrial atmosphere and stratospheric photochemical loss is one of its major sinks as a consequence of its slow oxidation rates in the troposphere (42). OCS is photolyzed in the high stratosphere (>25 km above sea level), oxidized to SO_2, and serves as an embedded SO_2 stratospheric source at those high altitudes. Shortly after SO_2 production it is photolyzed and oxidized to sulfates, which acquire large sulfur MIF signatures as observed at the South Pole after prolonged wildfires due to extremely dry weather ensuing the 1997–1998 super El Niño–Southern Oscillation (ENSO) (11). Although $\Delta^{33}S$ values in the South Pole ENSO record are positive (11), we do not rule out the possibility that this pathway may provide a consistent source of isotopically anomalous sulfates and contribute in part to the observed negative $\Delta^{33}S$ values because the Himalayas are likely a global hotspot for stratospheric intrusions (18, 19) and $\Delta^{33}S$ values in the stratosphere are spatially and temporally heterogeneous (14, 43). It has been observed that volcanic plumes produced varying MIF signatures (in sign and magnitude) over time as the plume photochemically evolves isotopically during long-range transport of sulfur compounds (14). The detailed chemistry and transport mechanism between the stratosphere and troposphere is particularly complex for the HTP (44–47), especially in the vicinity of Mt. Everest, and requires further modeling in the future. To improve and constrain such models, field-based measurements of quadrupole stable sulfur isotopes and biomass-burning tracers at varying locations including emission sources and background receptors become important. We also note that laboratory experiments of OCS photolysis (48) show slightly negative $\Delta^{33}S$ values (minimum: −0.23‰) in the produced elemental sulfur (Fig. 1), which may be oxidized to sulfate in today's oxygen-rich atmosphere. The negative $\Delta^{33}S$ values in the OCS photodissociation may be too small to contribute to our observed anomalies, but its role should not be neglected and further laboratory and field investigations are required.

Because deposition of isotopically anomalous sulfates of stratospheric volcanic origins occurs within several years after eruptions (11, 14), stratospheric volcanic events (e.g., Tambora in 1815, Cosigüina in 1835) only play a minor role, if any, in contributing to the most negative $\Delta^{33}S$ value observed from ~1818 to ~1853.

Comparison with Archean Barite Records and Possible Biogeochemical Implications

The sulfur isotopic anomaly in Archean (~4 to ~2.5 Ga) sediments is strong evidence of an anoxic atmosphere and a proxy for understanding the evolution of atmospheric oxygen and early life on primitive Earth (49), but corresponding biogeochemical processes are not fully understood (11). An interesting facet of our data is that the unique $\Delta^{33}S$–$\delta^{34}S$ pattern in the pre-1930 period is similar to published Archean barite ($BaSO_4$) data (Fig. 4), although the magnitude of $\Delta^{33}S$ is smaller because present-day sediments contain a large amount of isotopically normal sulfates. Archean barites are only observed in a relatively short period (3.5–3.2 Ga) and are characterized by a narrow range of positive $\delta^{34}S$ values (from ~3‰ to ~11‰) and negative $\Delta^{33}S$ values of -0.75 ± 0.39‰ ($n = 224$) (50–58), notably different from the Archean pyrite (FeS_2) and sulfide (S^{2-}) records ($-40‰ \le \delta^{34}S \le 25‰$; $-4‰ \le \Delta^{33}S \le 15‰$) (32). It has been a mystery why the oxidized form of sulfur can exsit in the anoxic atmosphere and its unique isotopic composition may represent a combined result of atmospheric, oceanic, and microbial processes (56). It is widely accepted that the Paleoarchean (3.6–3.2 Ga) was strongly affected by active volcanism (59) and negative $\Delta^{33}S$ values in barite deposits is likely an isotopic fingerprinting that sulfate is produced from photolytic reactions of SO_2 allowed by an anoxic atmosphere at that time (50–58). However, the deviation of $\delta^{34}S$ from the expected photochemical array is debated and explained by various concept models such as microbial sulfate reduction

(54), different atmospheric composition (i.e., wavelength-dependent MIF effects) (56), and/or mixing of varying sulfur reservoirs (52).

Our observation of Paleoarchean-barite-like $\Delta^{33}S$–$\delta^{34}S$ pattern in an oxygen-rich atmosphere (Fig. 4) implies that basic reactions responsible for sulfur MIF in combustion as discussed previously may also occur in the Paleoarchean. Although biomass burning is not possible, it is plausible, and cannot be ruled out, that recombination reactions of elemental sulfur (33) may be significant in the active Paleoarchean volcanism because formation of elemental sulfur related to volcanism are commonly observed on both Earth (60) and extraterrestrial bodies such as Io (61). Therefore, the negative ^{33}S anomalies in Paleoarchean barites produced in the volcano plume could in fact come from a strictly thermal reaction instead of photolytic reactions, which may yield different $\Delta^{33}S$–$\delta^{34}S$ patterns. In addition, OCS is a potentially important chemical component in the Archean atmosphere, for not only its role in photochemically produced sulfur isotopic anomalies (11, 56, 62), but also its greenhouse effect in solving the faint young sun paradox (62). Our long-term sulfur isotopic measurements in a high-altitude nonpolar region across the Anthropocene further support recent interpretations that OCS may be another possible sulfur-bearing molecule for producing isotopically anomalous sulfates in the present-day and possibly Archean atmospheres (11, 56).

Conclusions

In summary, our measurements of multiple stable sulfur and lead isotopes, major, trace, and rare earth elements in a two-century Himalayan sediment record suggest that the observed changes in sulfur cycling at the second industrial revolution reflects more dust-associated sulfates and climate-induced weathering/erosion affecting the Himalayas in the last century than the nineteenth century.

Dust-associated sulfates have acquired significant attention because of their ability to alter physical/chemical properties of other mineral components in the dust and relevant impacts on climate and ecosystems (26, 63). The Himalayan sulfur isotopic record provides an independent marker of anthropogenic-induced changes in the atmospheric composition and may help to improve our understanding of how historical and future changes in the coupling of sulfur and dust emissions affect radiative forcing, glacier surface albedo, and snow/glacier melting over the HTP (64–66). The discovery of enhancing weathering/erosion in this alpine glacial hydrological system in the past >100 y supports a recent 20-y investigation of water chemistry over the Himalayas (30), provides context for quantifying and projecting how such fragile ecosystems response to climate change, and may also have potentially important implications for other temperate glacial hydrological systems.

Additionally, our study highlights the need for better source apportionment of combustion-associated sulfur isotopic anomalies (such as fuels, OCS photolysis, or potentially underappreciated reactions during combustion) and quantifying their influences on $\Delta^{33}S$ and $\Delta^{36}S$ signatures in the present-day atmosphere. Given that chemical reactions responsible for sulfur MIF might have occurred throughout Earth's history (56), a complete understanding of sulfur MIF in the present-day atmosphere may be an important ingredient for further defining the relative roles of the dynamics, atmospheric chemistry, and microbial metabolisms on the formation and preservation of barites in the Paleoarchean.

Materials and Methods

TSP and glacier snow samples were collected at Nam Co Lake and Mount Everest, respectively (*SI Appendix*, Fig. S1). The sediment core was drilled at the Gokyo lake system (the world's highest oligotrophic freshwater lake system, ~4,800 m above sea level, ~15 km from the peak of Mount Everest) and dated by Kang et al. (3). The isotope ratios of quadruple sulfur isotopes (^{32}S, ^{33}S, ^{34}S, and ^{36}S) defined as $\delta^{3}xS=[(^{3}xS/^{32}S)_{sample}/(^{3}xS/^{32}S)_{VCDT}-1]*1{,}000$ (unit: ‰), where $x = 3$, 4, and 6 and VCDT stands for the Vienna Canyon Diablo Troilite reference material, were determined in the Stable Isotope Laboratory at University of California, San Diego, using the traditional BrF_5 fluorination method (8, 11, 12, 50) and an isotope ratio mass spectrometry (Thermo Finnigan MAT 253). A laboratory Ag_2S standard of approximately the sample sizes comparable to environmental samples (1–6 μmol) was subjected to the same analytical procedure throughout the study period to determine overall uncertainties of measurements (associated with extraction, fluorination, purification and mass-spectrometry measurements) (*SI Appendix*, Table S1). For large sizes of samples (>2.5 μmol), the errors (one SD) for $\delta^{34}S$, $\Delta^{33}S$, and $\Delta^{36}S$ values were less than 0.4‰, 0.01‰, and 0.1‰, respectively. The $\Delta^{36}S$ values in Mt. Everest samples are not reported in this study because of relatively large uncertainties associated with small sample sizes. The slightly greater SDs of $\delta^{34}S$ and $\Delta^{33}S$ (1.0‰ and 0.02‰, respectively) for small sizes of samples (<2.5 μmol) would not affect our interpretation and conclusion. Elemental and stable lead isotopic analysis was carried out in the Trace Element Laboratory at Academia Sinica using the microwave digestion method and an inductively coupled plasma mass spectrometry (Perkin-Elmer Elan 6100). Detailed information of sampling sites, sampling, chemical processing, quality assurance/control procedures, and PMF modeling approach can be found in *SI Appendix*. All stable sulfur isotope data reported in this study is available in *SI Appendix*, Tables S2 and S3.

ACKNOWLEDGMENTS. The authors thank Teresa Jackson, Shuen-Hsin Lin, Yi-Tang Huang, and Cheng-Ming Chou for technical assistance in isotopic and chemical analysis; Qianggong Zhang for scientific discussion on the hydrology of the Gokyo Lake; Chhatra Sharma for collecting lake sediment samples; and two anonymous reviewers for their constructive comments that significantly helped to improve the manuscript. Special thanks are due to Yanan Shen's group and the late Chih-An Huh for many interesting conversations on isotope biogeochemistry. M.L. acknowledges fellowships from the Guangzhou Elite Project (JY201303) and the visiting scholar program of Academia Sinica. This study was partially funded by National Natural Science Foundation of China Grants 41630754 and 41721091.

1. Zhisheng A, Kutzbach JE, Prell WL, Porter SC (2001) Evolution of Asian monsoons and phased uplift of the Himalaya-Tibetan Plateau since Late Miocene times. *Nature* 411:62–66.
2. Thompson LG, et al. (2000) A high-resolution millennial record of the South Asian monsoon from Himalayan ice cores. *Science* 289:1916–1920.
3. Kang S, et al. (2016) Atmospheric mercury depositional chronology reconstructed from lake sediments and ice core in the Himalayas and Tibetan Plateau. *Environ Sci Technol* 50:2859–2869.
4. Grigholm B, et al. (2015) Twentieth century dust lows and the weakening of the westerly winds over the Tibetan Plateau. *Geophys Res Lett* 42:2434–2441.
5. Kaspari S, et al. (2009) Recent increases in atmospheric concentrations of Bi, U, Cs, S and Ca from a 350-year Mount Everest ice core record. *J Geophys Res Atmos* 114:D04302.
6. Immerzeel WW, van Beek LPH, Bierkens MFP (2010) Climate change will affect the Asian water towers. *Science* 328:1382–1385.
7. Li C, et al. (2016) Sources of black carbon to the Himalayan-Tibetan Plateau glaciers. *Nat Commun* 7:12574.
8. Romero AB, Thiemens MH (2003) Mass-independent sulfur isotopic compositions in present-day sulfate aerosols. *J Geophys Res Atmos* 108:4524.
9. Guo ZB, et al. (2010) Identification of sources and formation processes of atmospheric sulfate by sulfur isotope and scanning electron microscope measurements. *J Geophys Res Atmos* 115:D00K07.
10. Han X, et al. (2017) Multiple sulfur isotope constraints on sources and formation processes of sulfate in Beijing PM2.5 aerosol. *Environ Sci Technol* 51:7794–7803.
11. Shaheen R, et al. (2014) Large sulfur-isotope anomaly in nonvolcanic sulfate aerosol and its implications for the Archean atmosphere. *Proc Natl Acad Sci USA* 111:11979–11983.
12. Lee CCW, Savarino J, Cachier H, Thiemens MH (2002) Sulfur (S-32, S-33, S-34, S-36) and oxygen (O-16, O-17, O-18) isotopic ratios of primary sulfate produced from combustion processes. *Tellus B* 54:193–200.
13. Harris E, Sinha B, Hoppe P, Ono S (2013) High-precision measurements of (33)S and (34)S fractionation during SO2 oxidation reveal causes of seasonality in SO2 and sulfate isotopic composition. *Environ Sci Technol* 47:12174–12183.
14. Baroni M, Thiemens MH, Delmas RJ, Savarino J (2007) Mass-independent sulfur isotopic compositions in stratospheric volcanic eruptions. *Science* 315:84–87.
15. Sharma CM, et al. (2012) First results on bathymetry and limnology of high-altitude lakes in the Gokyo Valley, Sagarmatha (Everest) National Park, Nepal. *Limnology* 13:181–192.
16. Holmer M, Storkholm P (2001) Sulphate reduction and sulphur cycling in lake sediments: A review. *Freshw Biol* 46:431–451.
17. Kang SC, Chen PF, Li CL, Liu B, Cong ZY (2016) Atmospheric aerosol elements over the Inland Tibetan Plateau: Concentration, seasonality, and transport. *Aerosol Air Qual Res* 16:789–800.

18. Lin M, et al. (2016) Resolving the impact of stratosphere-to-troposphere transport on the sulfur cycle and surface ozone over the Tibetan Plateau using a cosmogenic S-35 tracer. *J Geophys Res Atmos* 121:439–456.
19. Skerlak B, Sprenger M, Wernli H (2014) A global climatology of stratosphere-troposphere exchange using the ERA-Interim data set from 1979 to 2011. *Atmos Chem Phys* 14: 913–937.
20. Liu B, et al. (2017) Background aerosol over the Himalayas and Tibetan Plateau: Observed characteristics of aerosol mass loading. *Atmos Chem Phys* 17:449–463.
21. Tan HB, et al. (2014) Lead isotope variability of fine-grained river sediments in Tibetan Plateau water catchments: Implications for geochemical provinces and crustal evolution. *Lithos* 190:13–26.
22. Cong ZY, et al. (2011) Trace elements and lead isotopic composition of PM10 in Lhasa, Tibet. *Atmos Environ* 45:6210–6215.
23. Zhang G, et al. (2017) Redox chemistry changes in the Panthalassic Ocean linked to the end-Permian mass extinction and delayed Early Triassic biotic recovery. *Proc Natl Acad Sci USA* 114:1806–1810.
24. Ono S, Wing B, Johnston D, Farquhar J, Rumble D (2006) Mass-dependent fractionation of quadruple stable sulfur isotope system as a new tracer of sulfur biogeochemical cycles. *Geochim Cosmochim Acta* 70:2238–2252.
25. Smith SJ, et al. (2011) Anthropogenic sulfur dioxide emissions: 1850-2005. *Atmos Chem Phys* 11:1101–1116.
26. Harris E, et al. (2013) Enhanced role of transition metal ion catalysis during in-cloud oxidation of SO2. *Science* 340:727–730.
27. Alexander B, et al. (2012) Isotopic constraints on the formation pathways of sulfate aerosol in the marine boundary layer of the subtropical northeast Atlantic Ocean. *J Geophys Res Atmos* 117:D06304.
28. Philip S, et al. (2017) Anthropogenic fugitive, combustion and industrial dust is a significant, underrepresented fine particulate matter source in global atmospheric models. *Environ Res Lett* 12:044018.
29. Rogora M, Mosello R, Arisci S (2003) The effect of climate warming on the hydrochemistry of Alpine Lakes. *Water Air Soil Pollut* 148:347–361.
30. Salerno F, et al. (2016) Glacier melting increases the solute concentrations of Himalayan glacial lakes. *Environ Sci Technol* 50:9150–9160.
31. Kaspar S, et al. (2008) Snow accumulation rate on Qomolangma (Mount Everest), Himalaya: Synchroneity with sites across the Tibetan Plateau on 50-100 year timescales. *J Glaciol* 54:343–352.
32. Ono S (2017) Photochemistry of sulfur dioxide and the origin of mass-independent isotope fractionation in Earth's atmosphere. *Annu Rev Earth Planet Sci* 45:301–329.
33. Babikov D (2017) Recombination reactions as a possible mechanism of mass-independent fractionation of sulfur isotopes in the Archean atmosphere of Earth. *Proc Natl Acad Sci USA* 114:3062–3067.
34. Thiemens MH, Heidenreich JE, 3rd (1983) The mass-independent fractionation of oxygen: A novel isotope effect and its possible cosmochemical implications. *Science* 219:1073–1075.
35. Gao YQ, Marcus RA (2001) Strange and unconventional isotope effects in ozone formation. *Science* 293:259–263.
36. Gardiner WC (2000) *Gas-Phase Combustion Chemistry* (Springer, New York).
37. Yan J, Yang J, Liu Z (2005) SH radical: The key intermediate in sulfur transformation during thermal processing of coal. *Environ Sci Technol* 39:5043–5051.
38. Bainssahota SK, Thiemens MH (1989) A mass-independent sulfur isotope effect in the nonthermal formation of S2f10. *J Chem Phys* 90:6099–6109.
39. Marlon JR, et al. (2008) Climate and human influences on global biomass burning over the past two millennia. *Nat Geosci* 1:697–702.
40. Pechony O, Shindell DT (2010) Driving forces of global wildfires over the past millennium and the forthcoming century. *Proc Natl Acad Sci USA* 107:19167–19170.
41. Cong Z, et al. (2013) Historical trends of atmospheric black carbon on Tibetan Plateau as reconstructed from a 150-year lake sediment record. *Environ Sci Technol* 47: 2579–2586.
42. Bruhl C, Lelieveld J, Crutzen PJ, Tost H (2012) The role of carbonyl sulphide as a source of stratospheric sulphate aerosol and its impact on climate. *Atmos Chem Phys* 12: 1239–1253.
43. Pavlov AA, Kasting JF (2002) Mass-independent fractionation of sulfur isotopes in Archean sediments: Strong evidence for an anoxic Archean atmosphere. *Astrobiology* 2:27–41.
44. Vernier JP, et al. (2013) Comment on "Large volcanic aerosol load in the stratosphere linked to Asian monsoon transport". *Science* 339:647.
45. Fromm M, Nedoluha G, Charvát Z (2013) Comment on "Large volcanic aerosol load in the stratosphere linked to Asian monsoon transport". *Science* 339:647.
46. Bourassa AE, et al. (2013) Response to comments on "Large volcanic aerosol load in the stratosphere linked to Asian monsoon transport". *Science* 339:647.
47. Bourassa AE, et al. (2012) Large volcanic aerosol load in the stratosphere linked to Asian monsoon transport. *Science* 337:78–81.
48. Lin Y, Sim MS, Ono S (2011) Multiple-sulfur isotope effects during photolysis of carbonyl sulfide. *Atmos Chem Phys* 11:10283–10292.
49. Lyons TW, Reinhard CT, Planavsky NJ (2014) The rise of oxygen in Earth's early ocean and atmosphere. *Nature* 506:307–315.
50. Farquhar J, Bao H, Thiemens M (2000) Atmospheric influence of Earth's earliest sulfur cycle. *Science* 289:756–759.
51. Bao HM, Rumble D, Lowe DR (2007) The five stable isotope compositions of Fig Tree barites: Implications on sulfur cycle in ca. 3.2 Ga oceans. *Geochim Cosmochim Acta* 71:4868–4879.
52. Ueno Y, Ono S, Rumble D, Maruyama S (2008) Quadruple sulfur isotope analysis of ca. 3.5 Ga Dresser Formation: New evidence for microbial sulfate reduction in the early Archean. *Geochim Cosmochim Acta* 72:5675–5691.
53. Shen Y, Farquhar J, Masterson A, Kaufman AJ, Buick R (2009) Evaluating the role of microbial sulfate reduction in the early Archean using quadruple isotope systematics. *Earth Planet Sci Lett* 279:383–391.
54. Roerdink DL, Mason PRD, Farquhar J, Reimer T (2012) Multiple sulfur isotopes in Paleoarchean barites identify an important role for microbial sulfate reduction in the early marine environment. *Earth Planet Sci Lett* 331:177–186.
55. Montinaro A, et al. (2015) Paleoarchean sulfur cycling: Multiple sulfur isotope constraints from the Barberton Greenstone Belt, South Africa. *Precambrian Res* 267: 311–322.
56. Muller É, Philippot P, Rollion-Bard C, Cartigny P (2016) Multiple sulfur-isotope signatures in Archean sulfates and their implications for the chemistry and dynamics of the early atmosphere. *Proc Natl Acad Sci USA* 113:7432–7437.
57. Muller E, et al. (2017) Primary sulfur isotope signatures preserved in high-grade Archean barite deposits of the Sargur Group, Dharwar Craton, India. *Precambrian Res* 295:38–47.
58. Busigny V, et al. (2017) Iron and sulfur isotope constraints on redox conditions associated with the 3.2 Ga barite deposits of the Mapepe Formation (Barberton Greenstone Belt, South Africa). *Geochim Cosmochim Acta* 210:247–266.
59. Philippot P, van Zuilen M, Rollion-Bard C (2012) Variations in atmospheric sulphur chemistry on early Earth linked to volcanic activity. *Nat Geosci* 5:668–674.
60. Kumar M, Francisco JS (2017) Elemental sulfur aerosol-forming mechanism. *Proc Natl Acad Sci USA* 114:864–869.
61. Spencer JR, Jessup KL, McGrath MA, Ballester GE, Yelle R (2000) Discovery of gaseous S2 in Io's Pele plume. *Science* 288:1208–1210.
62. Ueno Y, et al. (2009) Geological sulfur isotopes indicate elevated OCS in the Archean atmosphere, solving faint young sun paradox. *Proc Natl Acad Sci USA* 106:14784–14789.
63. Li W, et al. (2017) Air pollution-aerosol interactions produce more bioavailable iron for ocean ecosystems. *Sci Adv* 3:e1601749.
64. Sokolik IN, Toon OB (1996) Direct radiative forcing by anthropogenic airborne mineral aerosols. *Nature* 381:681–683.
65. Zhang YL, et al. (2017) Light-absorbing impurities enhance glacier albedo reduction in the southeastern Tibetan Plateau. *J Geophys Res Atmos* 122:6915–6933.
66. Duan J, et al. (2017) Weakening of annual temperature cycle over the Tibetan Plateau since the 1870s. *Nat Commun* 8:14008.